To appear in *Molecular Physics*
Vol. 00, No. 00, Month 2009, 1–23

RESEARCH ARTICLE

The influence of excluded volume and excess ion polarizability on the capacitance of the electric double layer

Geraint Minton[a] and Leo Lue[b*]

[a] *School of Chemical Engineering and Analytical Science, The University of Manchester, Oxford Road, Manchester M13 9PL, UK*; [b] *Department of Chemical and Process Engineering, University of Strathclyde, James Weir Building, 75 Montrose Street, Glasgow G1 1XJ, UK*

(*Received 00 Month 200x; final version received 00 Month 200x*)

We apply a modified Poisson-Boltzmann theory which permits ions of different sizes and excess polarizabilities to the study of these properties' effects on the differential capacitance of the electric double layer. For a planar electrode, we find an analytical expression for the differential capacitance, which is examined in the limits of low and high applied potential. In the low potential limit, a reduction of the solution relative permittivity caused by the ion polarizability causes the differential capacitance to decrease above a certain concentration, relative to the Gouy-Chapman-Stern theory. A similar effect is observed for the excluded volume, but only if the ions are of different sizes. In the high potential limit, the differential capacitance decreases inversely with the square root of the applied voltage. In a mixed electrolyte, asymmetries in both ion size and excess polarizability alter the surface adsorption of species: at high potentials, smaller ions displace larger ions and less polarizable ions displace more polarizable ions. The extent of the displacement agrees favorably with experimental data. A further consequence of this displacement is the appearance of a second peak in the differential capacitance, which is enhanced by excess ion polarizability.

Keywords: capacitance; excess ion polarizability; excluded volume; electric double layer; electrolyte

1. Introduction

A charged surface in contact with an electrolyte will attract counterions and repel co-ions from the bulk solution, creating a region of local counter-charge with a high electric field near the surface, known as the electric double layer (EDL). A key property of the EDL is its differential capacitance C_D, which relates the charge density Σ which accumulates on the surface due to a change in its potential ϕ_0:

$$C_D = \frac{d\Sigma}{d\phi_0} \tag{1}$$

The differential capacitance plays an important role in modelling a wide variety of processes, such as the motion of colloidal particles in an applied electric field [1] and the behavior electro-osmotic pumps [2], including the phenomena of flow reversal in AC electro-osmosis [3], and the regulation of ion transfer and ion selectivity across cell membranes [4] and nanoporous channels [5, 6]. It is relevant to the fields of biology, materials science, colloid science and the study of nano-fluidic devices. Additionally, C_D characterizes the intrinsic behavior of electrochemical energy storage and generation devices, such

*Corresponding author. Email: leo.lue@strath.ac.uk

ISSN: 00268976 print/ISSN 13623028 online

DOI: 10.1080/0026897YYxxxxxxxx
http://www.informaworld.com

as electrochemical supercapacitors, batteries and fuel cells, which either store energy in the high electric field of the EDL or in which the electrochemical reactions which drive the system occur inside an EDL. The form of the differential capacitance is crucial in determining the physical behavior of these processes.

In models for these phenomena, C_D typically forms part of a larger calculation, for example, serving as the boundary condition for the partial differential equations governing the flow of charge in the simulation of an electro-osmotic flow [7]. Consequently, a physically accurate and computationally inexpensive model for the differential capacitance is required. Because the dependence of C_D on the applied potential is dictated by the structure of the EDL, this requires a model for the electric double layer.

The classical description of the EDL is provided by Gouy and Chapman [8, 9], who introduced the idea of the diffuse double layer, in which counter-ions from the electrolyte are attracted to the surface and co-ions are repelled from it. Under the assumption that the ions are point-like charges, the equilibrium double layer follows a Poisson-Boltzmann distribution. This is known as the Gouy-Chapman (GC) model. Stern later modified the model to account for the ion size by including an inner layer [10] into which ions cannot enter. This Stern layer sets a minimum approach distance for the charges to the surface. The Gouy-Chapman-Stern (GCS) model accurately describes the differential capacitance for low concentration electrolytes at low potentials. However, above the thermal voltage ($k_BT/e_0 = 25\,\mathrm{mV}$, where k_B is the Boltzmann constant, T is the temperature, and e_0 is the fundamental unit of charge) and for higher bulk concentrations, it is unable to explain many experimental observations. Despite its shortcomings, the GCS model is widely used for interpreting experimental data and understanding the microscopic behavior of electrode/electrolyte systems, in part because it can be evaluated relatively easily and is reasonably accurate for low concentrations and low potentials.

The GCS theory breaks down partly because it does not account for non-electrostatic interactions between the ion species in the system (i.e. interactions which are not purely Coulombic in nature). These interactions add an additional cost for ions to enter the double layer, which can be large enough so as to effectively limit the counter-ion concentration. One important effect that is missing from the GCS theory is excluded volume interactions (EVI), which capture the fact that ions have a physical size. Bikerman [11] first accounted for this within the context of the Poisson-Boltzmann theory using a lattice gas approach which limits the counter-ion concentration and therefore prevents the unrealistically high counter-ion surface concentrations of the GCS model. This model was later independently re-derived by several authors (see Ref. 12 for a detailed history).

Accounting for the EVI does lead to an explanation for, and in some cases quantitatively accurate agreement with, the experimental trends seen in the differential capacitance [13–21], as well as a number of other experimental observations. Essentially, excluded volume interactions limit counter-ion absorption, and therefore, the charge density in the EDL, causing a thickening of the double layer once the surface is saturated. It can also explain the ion selectivity in porous membranes [5, 6], the high frequency flow reversal seen in ACEO experiments [3], and the migration behavior of colloidal particles suspended in electrolytes [1]. However, in many cases, in order to quantitatively fit experimental measurements, it is necessary to use ion diameters that are much larger than the accepted hydrated diameters. This implies that other effects do play a significant role.

Besides excluded volume interactions, there has been recent interest in the influence of ion-solvent interactions on the EDL structure and, consequently, the differential capacitance. The permittivity of a bulk electrolyte, which is a measure of the tendency of the constituent solvent dipoles to align against, and thereby resist, an externally applied field, is known to decrease with increasing ion salt concentration [22]. The reasons for this are two-fold: (i) ions simply displace solvent molecules, leaving fewer dipoles per unit volume, and (ii) solvent molecules in the ion solvation shells preferentially align with the

strong ionic electric fields, reducing their ability to align to an applied field [23]. Since the permittivity of the solvated ions is typically lower than for the bulk solvent, increasing the ion concentration reduces the permittivity of the solution. The extent to which an ion reduces the solvent permittivity is related to its excess polarizability, which is typically larger for smaller or more highly charged ions.

In addition to modifying the permittivity of the solution, the excess polarizability also causes the electrochemical potential of the ions to grow quadratically with the electric field [24] for $|\phi'| < 0.25\,\mathrm{V\,nm^{-1}}$; for larger fields, dielectric saturation of the solvent causes the variation to become linear [11]. This growth in the species energy, due to the induced dipole on the ions in the high field region of the EDL, counterbalances the increased Coulombic force experienced by the counter-charge at high potentials, leading to dielectrophoretic saturation. As with the concentration limitation that results from the EVI, dielectrophoretic saturation has also been shown to cause the EDL to thicken at high potentials [23, 25–27]. The consequence of this is that excess ion polarizability is also able to explain the observed peaks in the differential capacitance curves [26].

Accounting for the changes to the solvent permittivity by treating ions as polarizable spheres has also recently been shown to improve the applicability of PB-type theories to divalent ions [28, 29], for which GCS theory is largely invalid, even at low potentials. Since these species have a very high excess polarizability, their strong interaction with the electric field in the EDL means that they experience a strong induction force, significantly limiting their concentrations in the EDL. A further consequence of the large interaction with the field is that monovalent ions, which have a much lower excess polarizability, are able to displace the divalent ions from a surface at high potentials.

In this work, we develop a simple approximate theory for electrolytes with ions of different diameters and excess polarizabilities, which is applicable to mixed electrolyte systems. This model is used to understand the influence and interplay of ion excluded volume and polarization on the differential capacitance of the EDL. The remainder of this paper is organized as follows. The mathematical description of the electrolyte system, which contains finite-sized, polarizable ions, is detailed in Section 2. The development of a simple local density functional theory to model the structure and thermodynamics of this system is also described in this section, along with a brief discussion of its limitations. In Section 3, this theory is then used to develop an analytical expression for the differential capacitance of an electrolyte solution near a planar electrode. We then investigate the low and high potential limits of the model. The predictions of the model are then compared to experimental data in Section 4, where we consider the trends in the physical and electrical properties of systems with asymmetric and mixed electrolytes. Finally, the main findings of this paper and directions for future work are summarized in Section 5.

2. Theory

We consider a general electrolyte comprised of ions immersed in a continuum solvent with a relative permittivity ε_w. Ions of type α have a charge q_α, solvated ionic diameter d_α, and excess polarizability χ_α. The EVI is described using a form of the van der Waals hard sphere model which permits ions of different sizes [30], while the polarization interaction is described using a linear approximation for point dipoles which has previously been outlined in the literature [23, 26].

2.1. *Excess ion polarizability*

When a polarizable ion is placed in an electric field, we model the induced charge as due to a point dipole $\boldsymbol{\mu}$ located at the center of the ion. For $|\phi'| \lesssim 0.25\,\mathrm{V\,nm^{-1}}$, to a good

approximation, the magnitude of the induced dipole can be considered proportional to the electric field [24]; therefore, we assume this to be the case and that the induced dipole is aligned parallel (or anti-parallel) to the electric field

$$\boldsymbol{\mu}_\alpha = -\chi_\alpha \nabla\phi(\mathbf{r}) \tag{2}$$

where χ_α is the excess polarizability in the region around ions of type α, values of which are listed for several species in Table 1.

Table 1. Hydrated ionic diameters [31], excess polarizabilities [22] and respective maximum concentrations for a selection of ionic species.

	d / nm	$c^{\max,\mathrm{vol}}$ / M	$4\pi\chi$ / M^{-1}	$c^{\max,\chi}$ / M^{-1}
cation				
H^+	0.564	9.26	-17	2.29
Li^+	0.764	3.71	-11	3.55
Na^+	0.716	4.52	-8	4.88
K^+	0.662	5.72	-8	4.88
Rb^+	0.658	5.83	-7	5.57
Cs^+	0.658	5.83		
Mg^{2+}	0.856	2.65	-24	1.63
La^{3+}	0.904	2.25	-35	1.11
anion				
F^-	0.704	4.76	-5	7.8
Cl^-	0.664	5.62	-3	13.00
I^-	0.662	5.72	-7	5.57
OH^-	0.600	7.69	-13	3.00
SO_4^-	0.758	3.81	-7	5.57

If the concentration distribution of ions in the system is $c_\alpha(\mathbf{r})$ through the system, then the associated charge density $Q(\mathbf{r})$ associated with these ions is

$$Q(\mathbf{r}) = \sum_\alpha q_\alpha c_\alpha(\mathbf{r}) + \sum_\alpha \chi_\alpha \nabla\phi(\mathbf{r}) c_\alpha(\mathbf{r}) \tag{3}$$

where we have used the fact that the charge density due to a point dipole $\boldsymbol{\mu}$ located at position $\mathbf{r}_0$ is $-\nabla\cdot\boldsymbol{\mu}\delta^3(\mathbf{r}-\mathbf{r}_0)$. The first term arises from the bare charge on the ions, while the second term is due to the induced charge on the ions. This assumes that the induced dipole density is proportional to the species concentration, which has been found to be a good approximation when $c_\alpha \lesssim 2\,\mathrm{M}$ [22].

2.2. *Mean-field approximation*

We now develop a simple description of the structure and thermodynamics of this system of polarizable ions. In this work, electrostatic interactions are treated using a mean-field approximation. Within this framework, the free energy functional F of a system of interacting charged particles is given by the expression [32]

$$F[c] = F^{\mathrm{ref}}[c] - \frac{1}{8\pi}\int d\mathbf{r}\,\varepsilon_w \nabla\phi(\mathbf{r})\cdot\nabla\phi(\mathbf{r}) + \int d\mathbf{r}\,[\Sigma(\mathbf{r}) + Q(\mathbf{r})]\,\phi(\mathbf{r}) \tag{4}$$

where $F^{\mathrm{ref}}[c]$ is the reference free energy functional for a system without electrostatic interactions, discussed below, $\phi(\mathbf{r})$ is the local electrostatic potential, and $\Sigma(\mathbf{r})$ is the fixed charge density (e.g., from an electrode).

By minimizing the free energy functional with respect to the electrostatic potential, we can determine its shape

$$\frac{\delta F}{\delta \phi(\mathbf{r})} = 0. \tag{5}$$

This leads to the Poisson equation

$$-\frac{1}{4\pi}\nabla \cdot [\varepsilon_w \nabla \phi(\mathbf{r})] = Q(\mathbf{r}) + \Sigma(\mathbf{r}). \tag{6}$$

The mobile charge density $Q(\mathbf{r})$ is composed of the sum of the bare charge located on each of the ions in the system and the induced charge on the ions, which is given by Eq. (3). Substituting this back into the Poisson equation, we can write

$$-\frac{1}{4\pi}\nabla \cdot [\varepsilon(\mathbf{r}) \nabla \phi(\mathbf{r})] = \sum_\alpha q_\alpha c_\alpha(\mathbf{r}) + \Sigma(\mathbf{r}). \tag{7}$$

where $\varepsilon(\mathbf{r})$ is a spatially varying relative permittivity of the solution, which depends on the local ion concentration as

$$\varepsilon(\mathbf{r}) = \varepsilon_w + 4\pi \sum_\alpha \chi_\alpha c_\alpha(\mathbf{r}) \tag{8}$$

The free energy functional of a solution of polarizable ions can be written in terms of the local relative permittivity $\varepsilon(\mathbf{r})$ as

$$F[c] = F^{\mathrm{ref}}[c] - \frac{1}{8\pi}\int d\mathbf{r}\, \varepsilon(\mathbf{r}) \nabla\phi(\mathbf{r}) \cdot \nabla\phi(\mathbf{r}) + \int d\mathbf{r} \left[\Sigma(\mathbf{r}) + \sum_\alpha q_\alpha c_\alpha(\mathbf{r})\right] \phi(\mathbf{r}). \tag{9}$$

Given an expression for the Helmholtz free energy functional, all thermodynamic properties of the system can be determined. For example, by taking the functional derivative of the free energy with respect to the concentration of species α gives the electrochemical potential μ_α of that species

$$\begin{aligned} \mu_\alpha(\mathbf{r}) &= \frac{\delta F[c]}{\delta c_\alpha(\mathbf{r})} \\ &= \mu_\alpha^{\mathrm{ref}}(\mathbf{r}; [c]) + q_\alpha \phi(\mathbf{r}) - \frac{\chi_\alpha}{2} |\nabla \phi(\mathbf{r})|^2 \end{aligned} \tag{10}$$

where $\mu_\alpha^{\mathrm{ref}}(\mathbf{r}; [c])$ is the chemical potential of species α in the absence of electrostatic interactions (i.e. in the reference system). As noted above, the quadratic dependence of μ_α upon the electric field holds for $|\phi'| \lesssim 0.25\,\mathrm{V\,nm^{-1}}$; for larger field strengths, the variation becomes linear [11], and so we expect this simple approximation for the electrochemical potential to breakdown.

2.3. *Reference system*

There are several different choices that can be used to model the free energy functional of the reference system. These range from using an ideal gas reference system to much more sophisticated and mathematically complex approximate density functional theories.

Within the local density approximation (LDA), we can write the reference component of the free energy functional as a function only of the local species concentrations:

$$F^{\text{ref}}[c] = \int d\mathbf{r} f^{\text{ref}}(c(\mathbf{r})) \tag{11}$$

where f^{ref} is the Helmholtz free energy density of a uniform reference fluid with species concentrations $c(\mathbf{r})$. This is comprised of an ideal (entropic) component and a residual component, which accounts for all non-electrostatic non-ideality. The use of the LDA can lead to artifacts in the prediction of the properties of the EDL [33]. While these are not significant at low concentrations and applied potentials, they can lead to qualitative inaccuracies at more severe conditions.

There are several models that can be used as the reference Helmholtz free energy. One popular choice is the Boublik-Mansoori-Carnahan-Starling-Leland (BMCSL) equation of state [34, 35], which accurately describes the thermodynamic properties of hard sphere mixtures. However, within the MF-LDA this is known to overestimate the influence of excluded volume effects at higher electrode potentials [36], due to the breakdown of the MF-LDA itself at high concentrations. As a result it is less accurate than simpler expressions, such as the lattice model used by Bikerman [11].

In this work, we also use a form of the van der Waals equation of state for mixed hard spheres, developed by Gorenstein *et al.* [30]. It is not limited to a single ion size, as in the Bikerman model, and provides a reasonable description of the excluded volume interaction in multicomponent systems. The reference free energy is given by

$$\begin{aligned} f^{\text{ref}}[c(\mathbf{r})] = k_B T \sum_\alpha c_\alpha(\mathbf{r})(\ln[c_\alpha(\mathbf{r})\Lambda_\alpha^3] - 1) \\ + k_B T \sum_\alpha c_\alpha(\mathbf{r}) \ln \frac{1}{1 - \sum_{\alpha'} c_{\alpha'}(\mathbf{r})\bar{v}_{\alpha'\alpha}} \end{aligned} \tag{12}$$

where Λ_α is the thermal wavelength of ions of type α. The denominator in the logarithm of the second term is the available volume fraction with respect to species α. The quantity $\bar{v}_{\alpha\alpha'}$ is defined as

$$\bar{v}_{\alpha\alpha'} = \frac{2v_{\alpha\alpha}v_{\alpha\alpha'}}{v_{\alpha\alpha} + v_{\alpha'\alpha'}}, \tag{13}$$

where $v_{\alpha\alpha'}$ is the excluded volume per ion between ions α and α', which we empirically modify from the original work by a factor of $\sqrt[3]{\frac{3}{2\pi}} \approx 0.78$ to define it in terms of the hydrated ion radii as

$$v_{\alpha\alpha'} = \frac{1}{8}(d_\alpha + d_{\alpha'})^3. \tag{14}$$

The modification is used to adjust the free energy density and maximum ion concentration to more closely resemble the Bikerman model. We henceforth refer to this as the modified van der Waals (mvdW) model. The corresponding electrochemical potential for this model is

$$\beta\mu_\alpha^{\text{ref}}(\mathbf{r}) = \ln\left[\frac{c_\alpha(\mathbf{r})\Lambda_\alpha^3}{1 - \sum_{\alpha'} c_{\alpha'}(\mathbf{r})\bar{v}_{\alpha'\alpha}}\right] + \sum_{\alpha'} \frac{c_{\alpha'}(\mathbf{r})\bar{v}_{\alpha\alpha'}}{1 - \sum_{\alpha''} c_{\alpha''}(\mathbf{r})\bar{v}_{\alpha''\alpha'}} \tag{15}$$

The first term in this expression is the same as that used by [29], but there is an addi-

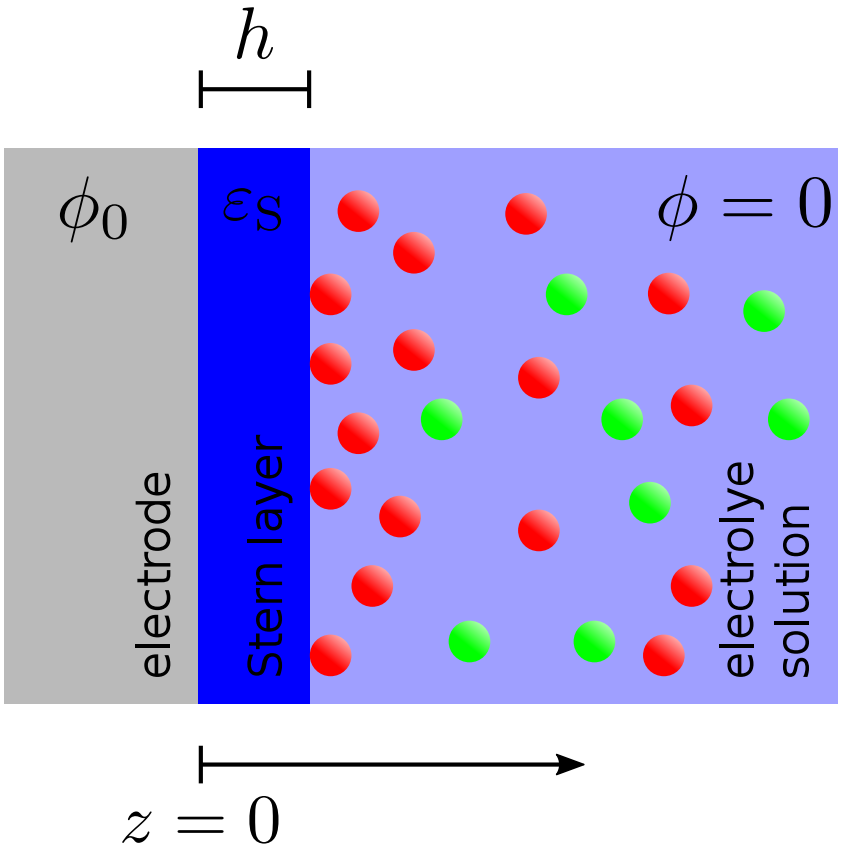

Figure 1. Schematic drawing of the planar electrode system studied in this work.

tional contribution from the second term. Measured values of the hydrated ionic diameter for the species described in this paper are shown in Table 1 along with the maximum concentration permitted by the mvdW model for that species, defined as

$$c_\alpha^{\max,\mathrm{vol}} = \frac{1}{8r_\alpha^3} = \frac{1}{\bar{v}_{\alpha\alpha}} \tag{16}$$

The corresponding expression for the pressure in this model is

$$\beta p^{\mathrm{ref}} = \sum_\alpha \frac{c_\alpha}{1 - \sum_{\alpha'} c_{\alpha'} \bar{v}_{\alpha'\alpha}} \tag{17}$$

3. Single planar electrode

Now we apply the theory described above to an electrolyte near a planar electrode with a Stern layer of thickness h and dielectric constant ε_S where ions cannot enter. The surface potential of the electrode is ϕ_0, and the potential of the electrolyte solution far from the electrode is taken to be equal to zero. The coordinate z measures the perpendicular distance from the surface of the electrode, and it is only along this coordinate that the properties of this system vary. A schematic representation of the system is shown in Fig. 1.

At equilibrium, the electrochemical potential should be constant in space, so we may

write

$$\mu_\alpha^{\mathrm{ref}}(c(z)) + q_\alpha\phi(z) - \frac{\chi_\alpha}{2}|\phi'(z)|^2 = \mu_\alpha^{\mathrm{ref}}(c(\infty)) \tag{18}$$

In this geometry, the Poisson equation is given by:

$$-\frac{1}{4\pi}[\varepsilon(z)\phi'(z)]' = \sum_\alpha q_\alpha c_\alpha(z) \tag{19}$$

By multiplying both sides of the Poisson equation by $\phi'(z)$ and integrating the result with respect to z, we find:

$$\frac{1}{4\pi}\left[\varepsilon(z) - \frac{\varepsilon_w}{2}\right]|\phi'(z)|^2 = p^{\mathrm{ref}}(c(z)) - p^{\mathrm{ref}}(c(\infty)) \tag{20}$$

where we have made use of the Gibbs-Duhem relation and the fact that $\phi'(z \to \infty) = 0$.

From Gauss' law, the surface charge Σ of the electrode can be directly related to the gradient of the electrostatic potential at both the surface of the electrode $z = 0$ and the outer edge of the Stern layer $z = h$:

$$\Sigma = -\frac{\varepsilon_{\mathrm{S}}}{4\pi}\phi'(0) = -\frac{\varepsilon(h)}{4\pi}\phi'(h) \tag{21}$$

The electrostatic potential at the outer edge of the Stern layer $\phi(h)$ can be directly related to the potential ϕ_0 of the surface of the electrode by noting that the electric field should be constant in the Stern layer:

$$\phi(h) = \phi_0 + \phi'(0)h = \phi_0 - \frac{4\pi\Sigma}{\varepsilon_{\mathrm{S}}}h \tag{22}$$

By applying these relations, we find

$$\mu_\alpha^{\mathrm{ref}}(c(h)) + q_\alpha\left(\phi_0 + \frac{4\pi\Sigma}{\varepsilon_{\mathrm{S}}}h\right) - \frac{\chi_\alpha}{2}\left|\frac{4\pi\Sigma}{\varepsilon(h)}\right|^2 = \mu_\alpha^{\mathrm{ref}}(c(\infty)) \tag{23}$$

$$\frac{1}{4\pi}\left[\varepsilon(z) - \frac{\varepsilon_w}{2}\right]\left|\frac{4\pi\Sigma}{\varepsilon(h)}\right|^2 = p^{\mathrm{ref}}(c(h)) - p^{\mathrm{ref}}(c(\infty)) \tag{24}$$

This provides a set of algebraic equations which can be solved to give the ion concentrations $c_\alpha(h)$ and the surface charge density Σ as a function of the electrode potential ϕ_0. These equations are much easier to solve than the Poisson equation (see Eq. (19)), which is a differential equation.

By taking the derivative of the surface charge density with respect to the applied voltage, we can develop an analytical expression for the differential capacitance C_D:

$$\frac{1}{C_D} = -\frac{4\pi\Sigma}{\varepsilon(h)\sum_\alpha q_\alpha c_\alpha(h)} + \frac{4\pi h}{\varepsilon_{\mathrm{S}}}$$

We will now examine the limiting cases of low and high applied potentials on the differential capacitance.

3.1. *Low potential limit*

At low values of the applied surface potential ϕ_0, we can expand the reference pressure p^{ref} to second order in the electrostatic potential, leading to an analytical expression for C_D at the point of zero charge (PZC):

$$\frac{1}{C_D} = \frac{4\pi\kappa^{-1}(h)}{\varepsilon(\infty)} + \frac{4\pi h}{\varepsilon_{\text{S}}} \tag{25}$$

where $\kappa(h)$ is the inverse Debye screening length at the outer edge of the Stern layer, given by

$$\kappa^2(h) = \frac{4\pi\beta}{\varepsilon(h)} \sum_{\alpha\alpha'} q_\alpha A^{-1}_{\alpha\alpha'} q_{\alpha'} \tag{26}$$

and $A_{\alpha\alpha'}$ is defined as

$$A_{\alpha\alpha'} = \frac{\delta_{\alpha\alpha'}}{c_\alpha} + \frac{\partial\beta\mu^{\text{res}}_\alpha}{\partial c_{\alpha'}} \tag{27}$$

where μ^{res}_α is the residual chemical potential of species α, the difference between the actual chemical potential and that of an ideal gas at the same temperature, volume, and species numbers. Equation (25) has the same form as in GCS theory, but the the inverse screening length is altered due to the effects of the excluded volume interactions and the additional concentration dependence of the permittivity due to ion polarizability.

For GCS theory $C_D \to \varepsilon_{\text{S}}/(4\pi h)$ as $c_\alpha \to \infty$. This behavior is unaffected by excluded volume interactions for identically sized ions, since, in this case, these do not alter the screening length at low potentials. Excluded volume interactions can, however, change the differential capacitance at the PZC for systems with ions of different size. This is shown in Fig. 2 for an electrolyte with a 0.8 nm cation and a selection of sizes of anion. Both species are assumed to be monovalent and the solvent permittivity is taken as $\varepsilon_w = 78$, the value for water at $T = 298$ K.

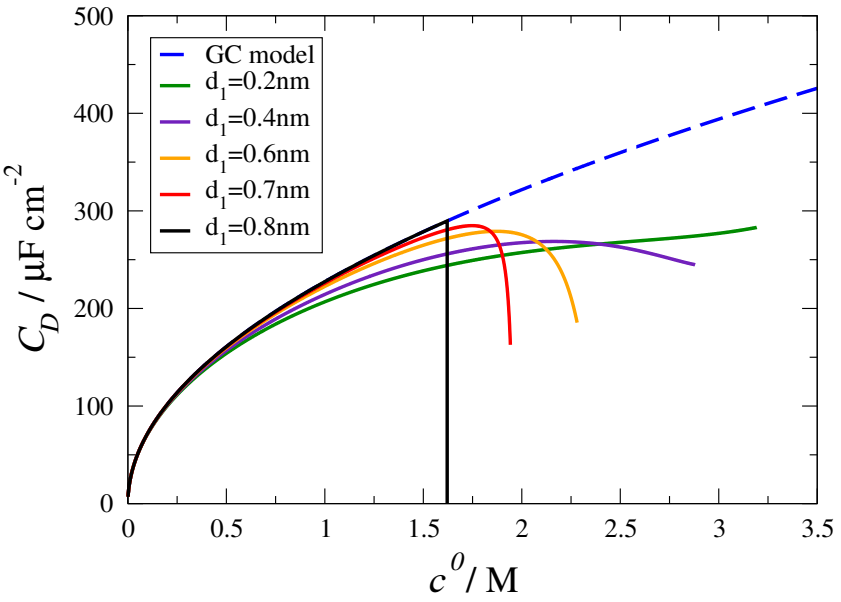

Figure 2. The dependence of the differential capacitance upon the concentration for a range of size-asymmetric electrolytes calculated using Eq. (26). The cation in all cases has diameter 0.8 nm, the anion diameter is listed as d_1 and the Stern layer width is zero.

Below the limit of the maximum bulk ion concentration, the model predicts no deviation from the GC model if the ions are equally sized, demonstrating that the excluded volume has no impact on the differential capacitance in this case. When there is an asymmetry in the ion size, C_D grows more slowly than predicted by the GC model, with larger asymmetries causing a slower growth. In all cases, C_D diverges at the maximum bulk concentration for that system, with the rate of divergence increasing as the asymmetry decreases, even while C_D tends towards the GC value.

While size asymmetry leads to a sizable reduction in the differential capacitance at larger concentrations and asymmetries, the concentration dependence of the permittivity which results from the ion polarizability has a larger effect over a much wider concentration range. In Fig. 3 we demonstrate this effect, plotting the solution of Eq. (25) at two different values of excess polarizability, assuming identical cations and anions. These curves are compared to both the GCS model and to experimental measurements of C_D at the PZC for ammonium nitrate and ethylammonium nitrate [37].

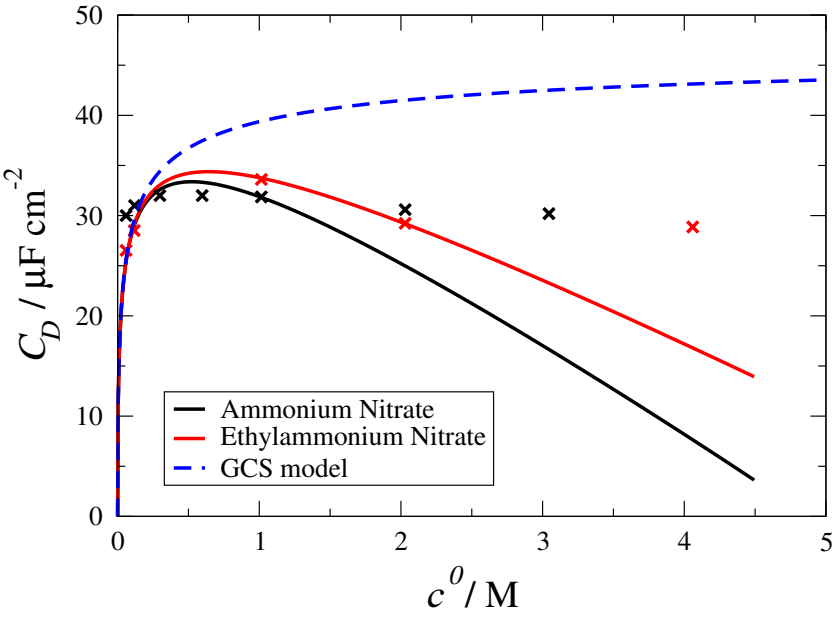

Figure 3. Comparison of analytical model for C_D at the PZC to the data in Ref. 37.

The model parameters (excess ion polarizabilities and Stern layer permittivity and width) were chosen to fit to the low concentration region of the experimental data, and take the values $h = 1.45\,\text{nm}$, $4\pi\chi_{AN} = -8\,\text{M}^{-1}$, $4\pi\chi_{EAN} = -6\,\text{M}^{-1}$ and $\varepsilon_\text{S} = \varepsilon(z = \infty)$. The GCS result, for which $\varepsilon(z) = \varepsilon_w$, assumes the same Stern layer width.

As with the effect of a small ion size asymmetry, accounting for the ion polarizability causes C_D to rise to a peak and then decay as the concentration increases but, in contrast, the peak occurs at a much lower concentration and the decay is much less precipitous. As a result, the predicted C_D deviates from the GCS model at a much lower concentration, and also has a concentration dependence which is much more similar to the experimental data. In particular, it is possible to attain reasonable quantitative agreement with experiment for concentrations up to between 1 to 2 M, using physically reasonable values for the ion excess polarizabilities (as compared to the measured values listed in Table 1). This would suggest that the polarizability interaction plays a significant role in determining the system properties at low potentials. With regards the large Stern layer width required for the fit, we note that it is not the width, but the ratio h/ε_S, that determines the effect of the Stern layer. Solvent molecules at an interface may be strongly aligned with the surface [38, 39], reducing the permittivity in the Stern layer, and accounting for this would lead to a smaller

width necessary to fit the data.

Regarding the deviation of the model from the measurement at high concentrations, we recall that this form of the polarizability interaction model, in which the permittivity varies linearly with concentration, is valid only for $c \lesssim 2\,\mathrm{M}$. At higher concentrations the permittivity decreases more slowly, which would shift the high concentration region of the model curves towards the experimental data, improving the fit.

3.2. *Large potential limit*

At large values of the applied potential, the co-ions are strongly depleted from the electrode and the counterions are strongly drawn to the electrode. In the Poisson-Boltzmann theory, there is no mechanism to limit this adsorption, and so the surface concentration of the counterions will exponentially increase with the applied electric potential. Physically, however, we have included in the theory two mechanisms that are able to counteract the adsorptions of the ions: negative ion polarizabilities and excluded volume interactions.

To examine this effect, we rewrite Eq. (18) as

$$\ln \frac{c_\alpha(z)}{c_\alpha(\infty)} = -\beta q_\alpha \phi(z) + \frac{\beta \chi_\alpha}{2} |\phi'(z)|^2 - \beta[\mu_\alpha^{\mathrm{res}}(c(z)) - \mu_\alpha^{\mathrm{res}}(c(\infty))] \tag{28}$$

In order that $c_\alpha(z)$ remain finite as $\phi(z) \to \infty$ (assuming that $q_\alpha < 0$), to leading order $\beta q_\alpha \phi(z)$ must be cancelled by either the polarization term or the residual chemical potential term. In the former case, the adsorption is controlled by polarization, while in the latter case, it is controlled by excluded volume.

Let us first consider a system where the counterion adsorption is physically limited by negative polarizabilities, rather than by ion size effects (i.e. $c_\alpha^{\max,\mathrm{vol}} > c_\alpha^{\max,\chi}$). For this system, we assume that all the ions have negative polarizabilities (i.e. $\chi_\alpha < 0$), in which case the adsorption is controlled by the counter-ion with the smallest value of χ_α/q_α , which we refer to as species A. Without loss of generality, we assume that the maximum value of the concentration of A will be $c_A^{\max,\chi}$.

We note from previous work [25, 26] that as $\phi \to \infty$ the ion polarizability limits the surface concentration of the counter-ion because the attractive electrostatic interaction is balanced against the unfavorable polarization interaction. In order for the concentration of species A to remain finite and constant as $\phi(z) \to \infty$, from Eq. (28) we require:

$$\phi'(z) \approx \left[-\frac{2}{\beta \chi_A} \left(\ln \frac{c_A(z)}{c_A(\infty)} + \beta \Delta \mu_A^{\mathrm{res}}(c(z)) + \beta q_A \phi(z) \right) \right]^{1/2}$$

The slope of the potential is dictated by the properties of counterion species A. While the entropic and residual chemical potential terms remain finite when evaluated at $c_A^{\max,\chi}$, their contribution can still be significant if $c_A^{\max,\mathrm{vol}} \approx c_A^{\max,\chi}$, such as for both Li^+ and I^-.

This variation of ϕ' implies that the concentration of all other counterion species with $\chi_\alpha/q_\alpha > \chi_A/q_A$ will vanish as $\phi(z) \to \infty$. Therefore, as shown in section 4.2, in the case where the polarizability controls the adsorption, there will only be one absorbed species on the electrode surface at high values of the applied potential.

The dielectric constant of the solution can be determined from Eq. (20)

$$\varepsilon(z) \approx \frac{\varepsilon}{2} + 2\pi\chi[p^{\mathrm{ref}}(c(z)) - p^{\mathrm{ref}}(c(\infty))] \left(\ln \frac{c_A(z)}{c_A(\infty)} + \beta \Delta \mu_A^{\mathrm{res}}(c(z)) + \beta q_A \phi(z) \right)^{-1}$$

Therefore, the dielectric constant of the solution will approach half the dielectric constant of the background solvent as $\phi(z) \to \infty$. In this limit, from the linear relation between

the ion concentration and the solution dielectric constant given in Eq. (8), the maximum concentration of ions is

$$c_A^{\max} = -\frac{\varepsilon}{8\pi\chi_A}. \tag{29}$$

as has been noted previously [26].

Finally, we note that the differential capacitance varies as

$$C_D \approx \frac{\varepsilon_w/2}{8\pi}\left[\frac{\chi_A}{2q_A^2}\left(\ln\frac{c_A(h)}{c_A(\infty)} + \beta\Delta\mu_A^{\rm res}(c(h)) + \beta q_A\phi(h)\right)\right]^{-1/2} + \cdots \tag{30}$$

where we have used the fact that to this level of approximation, the difference in the potential at the electrode and the outer surface of the Stern layer is negligible.

In the high potential region, the differential capacitance decreases at a rate proportional to $\phi_0^{-1/2}$, independently of the bulk electrolyte concentration, in agreement with experiment and simulation [15, 40, 41] and a property which has been described as a universal consequence of ion crowding near to a charged surface [1].

Now we examine the case where excluded volume effects control the counterion adsorption. This occurs when the maximum concentration of the counterions allowed by packing is less than that allowed by polarizability effects (i.e. $c_\alpha^{\max,\rm vol} < c_\alpha^{\max,\chi}$). From Eq. (28), we find in this situation that the residual chemical potential of each ion species must diverge as

$$\mu_\alpha^{\rm res}(c(z)) \approx -q_\alpha\phi(z) + \frac{\chi_\alpha}{2}|\phi'(z)|^2 + \cdots$$

The variation of ϕ' with the electrostatic potential can be deduced from Eq. (20):

$$|\phi'(z)|^2 = 4\pi\frac{p^{\rm ref}(c(z)) - p^{\rm ref}(c(\infty))}{\varepsilon(z) - \varepsilon/2}$$

We expect that $|\phi'(z)|$ will vary linearly with the electrostatic potential, which is consistent with a linear divergence of the pressure with $\phi(z)$. By combining these facts with the Gibbs-Duhem equation, we find the following expansions

$$\mu_\alpha^{\rm res}(c(z)) \approx -\left[q_\alpha + \frac{8\pi}{\varepsilon(z)}\sum_{\alpha'} q_{\alpha'}c_{\alpha'}(z)\right]\phi(z) + \cdots \tag{31}$$

$$p^{\rm ref}(c(z)) \approx -\frac{2}{\varepsilon(z)}[\varepsilon(z) - \varepsilon/2]\left[\sum_\alpha q_\alpha c_\alpha(z)\right]\phi(z) + \cdots \tag{32}$$

$$\phi'(z) \approx -\left[-\frac{8\pi\phi(z)}{\varepsilon(z)}\sum_\alpha q_\alpha c_\alpha(z)\right]^{1/2} + \cdots \tag{33}$$

The surface concentrations can be determined by solving the algebraic equations given in Eq. (31) and these values can then be used to determine the local dielectric constant of the solution $\varepsilon(h)$.

The differential capacitance is given by

$$C_D \approx \left[-\frac{\varepsilon(h)}{8\pi}\sum_\alpha q_\alpha c_\alpha\right]^{1/2}\phi_0^{-1/2} \tag{34}$$

As in the previous case, the differential capacitance decreases with the square root of the potential.

Comparison of the analytical and full numerical solutions is made in Fig. 4 for three cases, all with a bulk ion concentration of $0.01\,\mathrm{M}$ and with approximately the same maximum ion concentration of $4.85\,\mathrm{M}$. In the first case, only the polarizability is accounted for, with $4\pi\chi = -8\,\mathrm{M}^{-1}$, in the second only the EVI is accounted for, with $d = 0.7\,\mathrm{nm}$, and in the third case both properties are accounted for. The Stern layer width in all cases is zero.

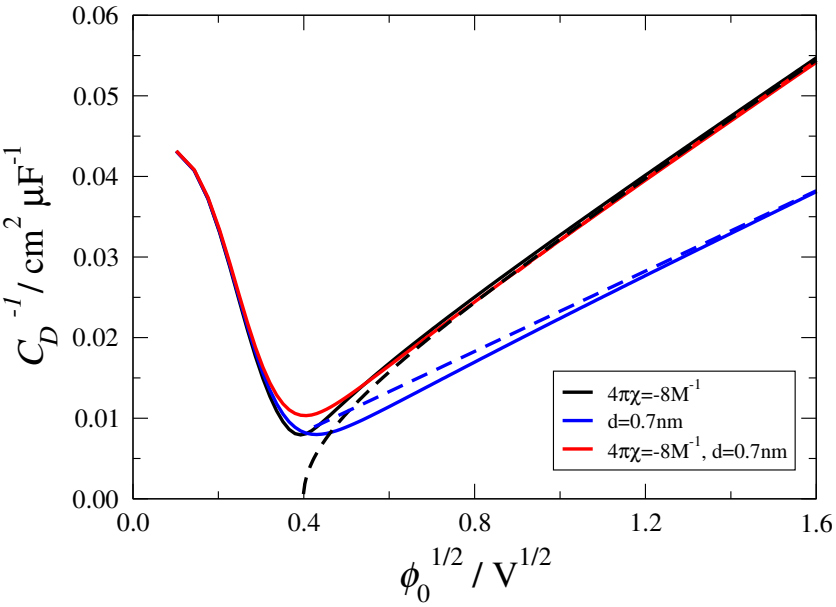

Figure 4. Calculated differential capacitance from the full model (solid lines) and the high potential approximations (dashed lines). Three cases are shown: with only the polarizability interaction (black), with only the EVI (blue) and with both (red). In all cases $c^{\max} \approx 4.85\,\mathrm{M}$.

For the cases in which the polarizability defines $c^{\max}$ (with or without the EVI term) there is good agreement between the full solution and the analytical expression given in Eq. (30). When the EVI defines the maximum concentration, the low order approximation given in Eq. (34) results in the correct trend but underestimates the actual value to a small degree at high potentials, indicating that higher order corrections are required. The effect of the polarizability interaction is clear, however, causing the differential capacitance to decay at a faster rate than the EVI alone. The reason for this is that, despite both systems having the same amount of counter-charge at the interface (since the surface is saturated in the high-potential region), the reduced permittivity that results from the inclusion of the polarizability interaction means that the structure of the rest of the EDL differs. In particular, the amount of counter-charge contained in the EDL is smaller, as is the the rate at which the counter-charge grows when the potential is increased.

4. Results and discussion

4.1. *Single electrolytes*

Experimental data for the differential capacitance of aqueous solutions of KPF_6 at the 110 surface of a silver electrode [42] are shown in Fig. 5, for electrolyte concentrations of 5 mM and 0.1 M. Overlaid on this are the predictions of the model with ion polarizability and the mvdW and BMCSL models to describe the EVI. Since the solvated diameter and excess polarizability of the PF_6^- ion are unknown, in both models these values have been

set equal to the measured values of the K^+ ion, shown in Table 1. The permittivity of the Stern layer is set equal to the value at $z = h$, so is a function of the surface concentration according to Eq. (8), while the the Stern layer width is used as a fitting parameter, in all cases taking the value $h = 0.44$ nm.

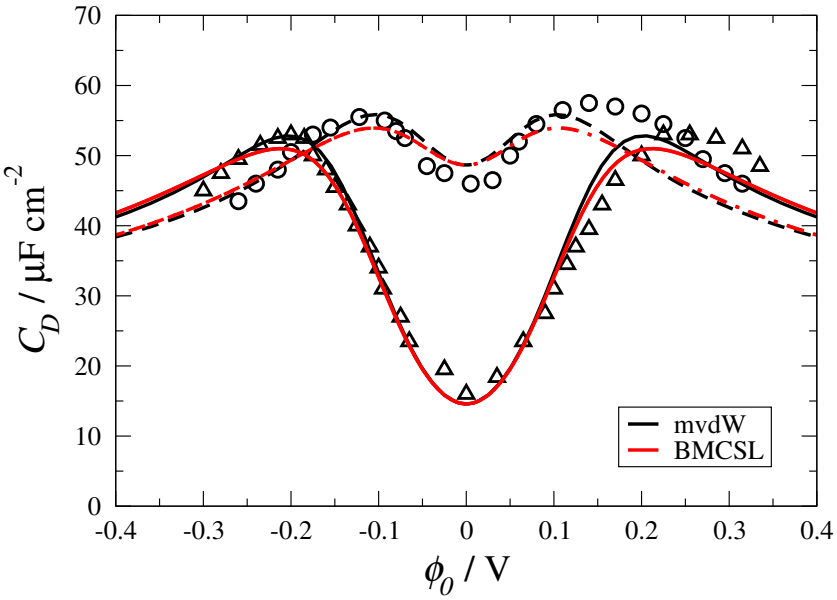

Figure 5. Comparison of the mvdW and BMCSL model predictions to experimental data for a KPF_6 electrolyte [42] when the polarizability interaction is also accounted for. Both ions take the parameters of the K^+ ion, listed in Table 1. Solid lines/triangles indicate the model solutions and experimental data for a 5 mM electrolyte and dashed lines/circles indicate the model solutions and experimental data for a 0.1 M electrolyte

In the negative potential region, where the K^+ ion forms the adsorption layer, the mvdW model offers a slightly improved fit over the BMCSL model, with the latter underestimating the peak value of C_D at both concentrations and decaying slightly more slowly at higher potentials. Although not shown here, the quality of the fit of the mvdW model is similar to that of the Bikerman model when polarizability effects are accounted for [26], but the two models better describe different regions of the data: the former better estimates the magnitude of the peak C_D while the latter, although it overestimates the value at this point, decays more rapidly at larger potentials, in line with the experimental data for that region.

We also show, in Fig. 6, a comparison of the model prediction for the double layer capacitance of a NaF electrolyte at the 210 crystal face of a gold electrode. The hydrated ion diameters and excess polarizability are given in Table 1, the Stern layer permittivity is taken to be equal to the value at $z = h$ and the width was used as a fitting parameter across all electrolyte concentrations and applied potentials, taking the value $h = 0.59$ nm.

Qualitatively, the model correctly describes the trends for all concentrations and potentials, including the shift from two peaks to a single peak with increasing concentration, the order of the curves (at low potentials C_D increases with concentration, at high potentials it C_D decreases) and the relative shift of the central minimum/maximum away from $\phi_0 = 0$ at high concentrations.

While the model also provides a reasonable quantitative fit for $-0.15\,\mathrm{V} < \phi_0 < +0.15\,\mathrm{V}$ at all concentrations, there are two main deviations from the measured data. The first of these is the slower decay of C_D on either side of the peak(s). As shown in Fig. 4, ion polarizability tends to cause C_D to decay more rapidly at large potentials; indeed, the model prediction can be improved by increasing the ion polarizabilities and decreasing their diameters, possibly indicating that the polarizability interaction is underestimated in the model system. However, while this does lead to an improved fit to the data

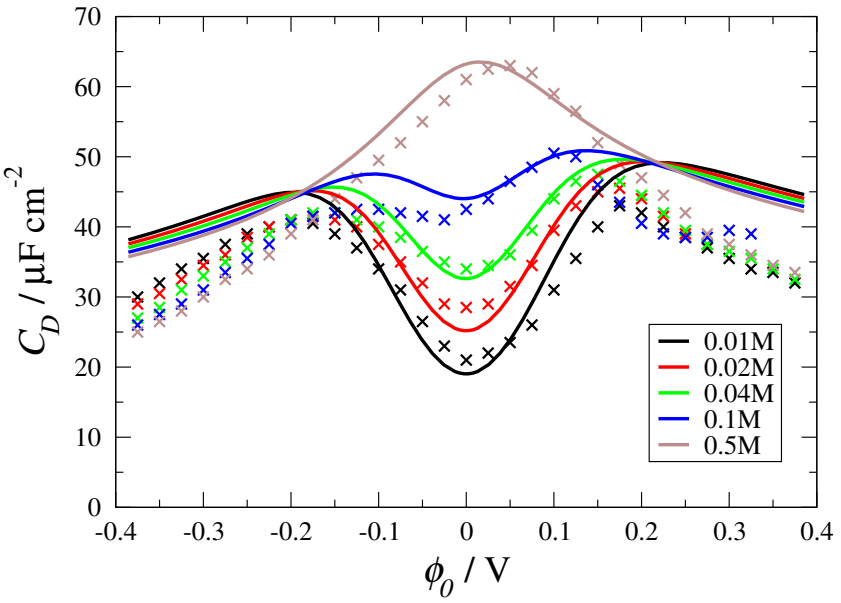

Figure 6. Comparison of model to experimental differential capacitance data for NaF electrolyte at an Au electrode with varying ion concentration. Solid lines are the model while crosses are experimental data [43].

at low potentials, even slightly extending the range of validity of the model, it is ultimately the case that the experimental C_D decays more rapidly than predicted at larger potentials. More problematically, different fit parameters are required at different concentrations, and the parameters which best describe the low (high) concentration case give a significantly worse fit of the high (low) concentration data than when the measured parameter values are used.

The second deviation can be seen in the offset from 0 V of the peak differential capacitance for the 0.5 M electrolyte. This does not occur because the differential capacitance of 0.5 M F^- should be at $\phi_0 > 0$ V: if the Na^+ ions had the same diameter and polarizability as the F^- ions, there would only be a single peak and it would be located at $\phi = 0$ V. Instead, within the confines of the model, this offset is defined by the asymmetry between the anions and cations, so is linked to the suppression of the differential capacitance at the PZC, discussed in Section 3.1. Specifically, when the concentration is large, an asymmetry of size or excess polarizability between the species in the system will cause the peak of the C_D curve to shift towards the concentration in which the smaller/lower polarizability species is the counter-ion.

The reason for the movement of the peak is that, at high concentrations, the larger/higher polarizability species is closer to its maximum concentration. The EVI/polarizability energy grows highly non-linearly as this limit is reached, so a small difference in ion sizes/polarizabilities can mean a large difference in the way the interaction energy grows as the EDL grows. Consequently, the growth of counter-charge in the EDL can depend strongly on the asymmetry between the ions, even near the PZC, leading to the observed changes in the differential capacitance.

The differences between the measured data and the model predictions imply that the interaction energies in the system are underestimated. At high potentials the energy cost for ions entering the double layer should grow more rapidly with the applied potential than it does in the model, so as to further suppress the growth in the surface charge density and reduce the differential capacitance. At low potentials, an additional energy difference between the co- and counter-ions would increase the offset of the peak of C_D. Such a difference does not have to arise from the interactions accounted for in the model; it could be the case that F^- ions interact more favorably with the surface than Na^+ ions, meaning they are more readily attracted into the EDL, for example.

4.2. *Mixed electrolytes*

4.2.1. EDL structure

We now apply the model to mixed electrolytes (i.e. those which contain more than one type of anionic and/or cationic species), where the EDL can be composed of more than one type of counter-ion. X-ray reflectivity measurements of the counter-charge at the surface of negatively charged Langmuir monolayers of behenyl sulphate [44] have shown that, at high surface charge densities, Cs^+ ions will displace both Li^+ ions and Mg^{2+} ions from the surface, when in equimolar solutions with each. GCS theory is unable to explain these observations: for a Cs^+-Li^+ mixture, it predicts equal surface concentrations, while for a Cs^+-Mg^{2+} mixture, it predicts a large excess of Mg^{2+} ions at the surface.

For the Cs^+-Li^+ system, a BMCSL-modified Poisson-Boltzmann model [12] and Monte Carlo simulations [45] both show that the difference between the sizes of ions can explain the experimental data: the smaller Cs^+ ions displace the larger Li^+ ions when the surface charge is high in order to minimize the energy of the system by allowing more counter-charge to approach the surface. However, the BMCSL model was unable to explain the Cs^+-Mg^{2+} data unless the diameter of the Mg^{2+} ion is increased by 20% over its physical value. Furthermore, while the Monte Carlo simulation compared significantly better, it still underestimated the amount of Cs^+ in the double layer by between 14% and 24%, and it was suggested that other factors, including polarization, may be significant [45].

Ion displacement due to EVI occurs because the smaller ion has a larger maximum concentration, thus giving a larger counter-charge concentration in the EDL at the surface. Ion polarizability, which also leads to a maximum concentration that differs between species, can cause the same effects in a mixed electrolyte. Figure 7 shows the ion concentration profiles at two applied potentials for three univalent mixed electrolytes in which the pairs of counter-ions have different polarizabilities. The bulk electrolyte in all cases consists of 5 mM of each counter-ion species and 10 mM of the co-ion. For simplicity in this hypothetical system, the Stern layer width is set to zero.

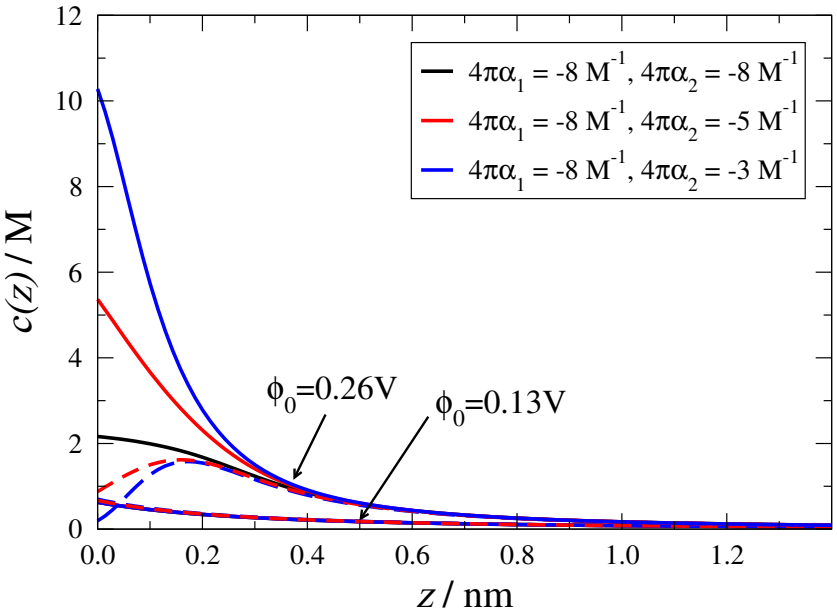

Figure 7. EDL structure for a mixed electrolyte at two electrode potentials when only the ion polarizability is accounted for and the two counter-ion species have different polarizability values, as labelled. Both species 1 (dotted lines) and species 2 (solid lines) have bulk concentrations of 5 mM.

Similarly to the case when only excluded volume is considered, at low applied poten-

tials the surface concentrations are approximately equal, but at higher potentials there is preferential adsorption of the species with the smaller value of χ_α/q_α. This is because these species experience a smaller induction force due to their weaker interaction with the large electric field near the surface, meaning that a larger surface counter-charge can be maintained through the displacement of the species with the higher χ_α/q_α ratio.

We now demonstrate that ion polarizability makes a considerable contribution to explaining the Cs^+-Mg^{2+} data described above. Defining the excess quantity of a species in the double layer, Γ_α, as

$$\Gamma_\alpha(\phi) = \int_0^\infty dz\,(c_\alpha(z) - c_\alpha^0), \tag{35}$$

Fig. 8 shows the fraction of Cs^+ ions which make up the total counter-ion concentration, calculated as $\Gamma_{Cs^+}/(\Gamma_{Cs^+} + \Gamma_{Mg^{2+}})$. Three sets of parameters are shown, as denoted by the line style. The dotted line is the Cs^+ fraction calculated assuming the all ion radii and excess polarizabilities listed in Table 1, except for the Cs^+ ion itself, for which the excess polarizability value is unknown. We use the value $4\pi\chi_{Cs^+} = -8\,\mathrm{M}^{-1}$, to be similar to that for other group I elements. The solid lines show the predicted Cs^+ fractions assuming a reduced Mg^{2+} polarizability of $4\pi\chi_{Mg^{2+}} = -21\,\mathrm{M}^{-1}$, and the dashed lines are the predictions of the GC, BMSCL and mvdW models in the absence of ion polarizability.

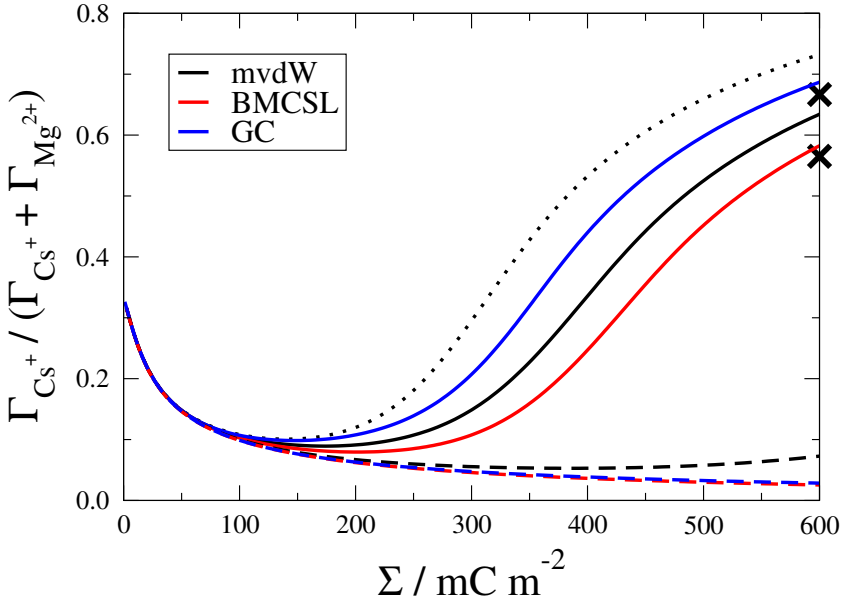

Figure 8. Ratio of total excess Cs^+ ions to the total number of excess counter-ions as a function of the surface charge density for a Cs^+-Mg^{2+} double layer. Marked crosses at $600\,\mathrm{mC\,m^{-2}}$ show the measured range of values from Ref. 44. Dashed lines show the results for the respective EVI theories alone, and solid and dotted lines show the same results but with the polarizability interaction included (see text for details)

It is immediately apparent that ion polarizability makes a significant contribution to the exclusion of Mg^{2+} from the EDL, to the extent that $\chi_{Mg^{2+}}$ must be reduced below its measured value in order to fit the experimental data. There are a number of possible reasons for this, but physically this can be justified (albeit empirically) by considering the limitations of the underlying model.

The assumption that the induced charge density of the solution is linearly dependent on the species concentration (see Eq. (3)) is only valid for concentrations up to $\sim 2\,\mathrm{M}$, above which the growth rate of the induced charge with concentration slows. Furthermore, the quadratic growth of the electrochemical potential with the electric field (see Eq. (10)) reduces to a linear growth for $|\phi'| > 0.25\,\mathrm{V\,nm^{-1}}$. The first point translates directly to

χ_α reducing at higher concentrations, while the second corresponds to a weakening of the interaction with the electric field at higher field strengths, both of which would result in a higher proportion of Mg^{2+} ions being in the EDL at higher surface charge densities.

Despite the limitations of the model used in this work, it is clear that ion polarizability plays a significant role in the EDL structure, particularly when higher-valency ions are involved in the system because these species interact strongly with both the electric field and the solvent. GCS theory breaks down entirely for such species, while EVI-only models are largely unable to correct the problems without inflating the ion radii in the EDL.

4.2.2. Differential capacitance

The displacement of one species by another can have a significant effect on the differential capacitance of EDL. To demonstrate this, we show in Fig. 9 the predicted differential capacitance of a NaCl-NaF mixed electrolyte, using the species diameter and polarizability values listed in Table 1 together with a Stern layer width of $h = 0.7$ nm. The choice of system reflects differential capacitance data available in the literature [46] for a NaCl-NaF electrolyte with a total ionic strength of 0.5 M but with Cl^- ion concentrations ranging from $4.5\,\mu$M to 17 mM.

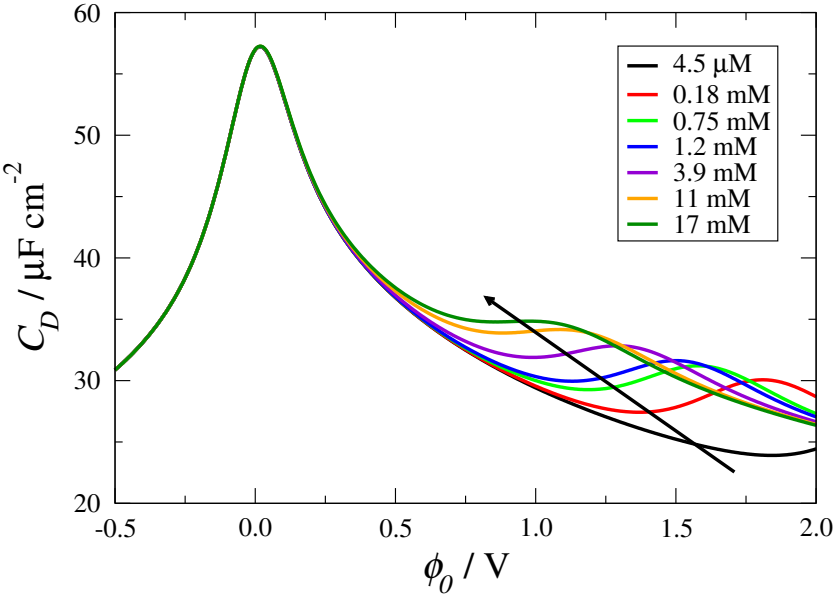

Figure 9. Predicted differential capacitance for a mixed NaF-NaCl electrolyte with a total ionic strength of 0.5 M but different proportions of of Cl^- ions.

At all Cl^- concentrations, the model predicts that C_D peaks at the PZC and decays identically in the negative potential region, where Na^+ is the counter-ion. For positive potentials, the curves decay in a similar manner for $\phi_0 \lesssim 0.5$ V but begin to diverge at larger potentials. For low Cl^- concentrations, there is a second peak in C_D which becomes larger and shifts to lower potentials as the Cl^- concentration increases, ultimately becoming a shoulder on the primary peak. Beyond the prediction of two peaks in the differential capacitance at approximately the correct order of magnitude in value, the model provides a poor fit to the experimental data due to differences in the relative sizes of the peaks and their separation. Possible reasons for this will be discussed in the following section, but the process by which the model suggests the second peak arises and the role played by the ion polarizability is of interest as it potentially contributes to the second peak and also highlights the complexities of such mixed electrolyte systems.

The origin of the second peak lies in the displacement of the larger, more polarizable

F^- ions by the smaller, less polarizable Cl^- ions; this can occur even when the bulk concentration of Cl^- is a very small fraction of the total anion concentration, resulting in the type of double layer structure shown in Fig. 7. However, this displacement alone is insufficient to cause a second peak in the differential capacitance for this system. This is demonstrated in Fig. 10, where we show a comparison of the mvdW, BMCSL and GCS models, each with and without ion polarizability, for the system with 17 mM Cl^- ions.

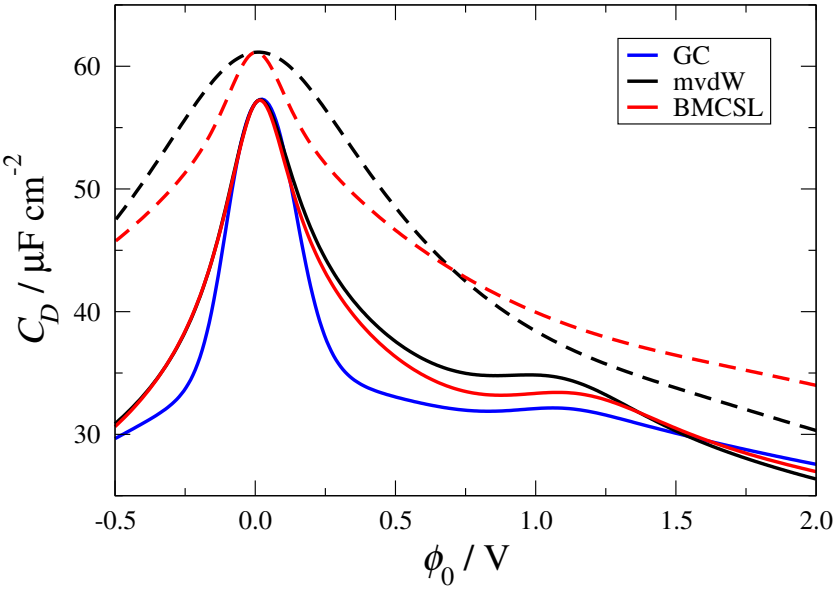

Figure 10. Predicted differential capacitance curves for the 17 mM case of Fig. 9 using the GC, mvdW and BMCSL models, with and without ion polarizability (solid lines and dashed lines, respectively).

In the EVI-only models, while the rate of decay of C_D at high potentials deviates slightly from being proportional to $\phi_0^{-1/2}$, as it is in the single electrolyte case, there is only a single peak. Ion polarizability causes more significant changes to the differential capacitance at high potentials. Ion polarizability alone results in a long shoulder on the main peak near the PZC, while the addition of EVI causes a broadening of the main peak and the smoothing of the shoulder region, although a clear imprint of the ion polarizability remains.

In general, the appearance of the shoulder/second peak is related to the displacement of one species by another. The process of displacement allows more counter-charge near the electrode surface, slowing the rate C_D decays or, if the asymmetry between the two counter-ion species is large enough, even allowing it to grow as ϕ_0 is increased. In the example considered here, the size asymmetry is relatively small between the two counter-ions, and it is the changes in permittivity which drive the appearance of the second peak.

In addition to having a smaller diameter than F^- ions, Cl^- ions also have a lower polarizability. As a result, when they displace the F^- ions at the surface, the permittivity near the surface increases, as can be seen in Fig. 11, which shows the permittivity at the Stern layer boundary ($z = h$) as a function of the applied potential for each of the data sets in Fig. 9.

This increase in the permittivity allows the electric field to grow faster with the potential, so the surface charge density is able to temporarily grow at a faster rate than it would if the permittivity remained constant (as in the EVI-only models) or if it reduced (i.e. if the Cl^- polarizability were larger than that of F^-). It can also be seen that, following the displacement of the F^- ions, the permittivity begins to decrease again, but only at a very low rate. This is due to the interplay between the excluded volume and ion polarizability, as described recently by Nakayama and Andelmann [27] for a single electrolyte system.

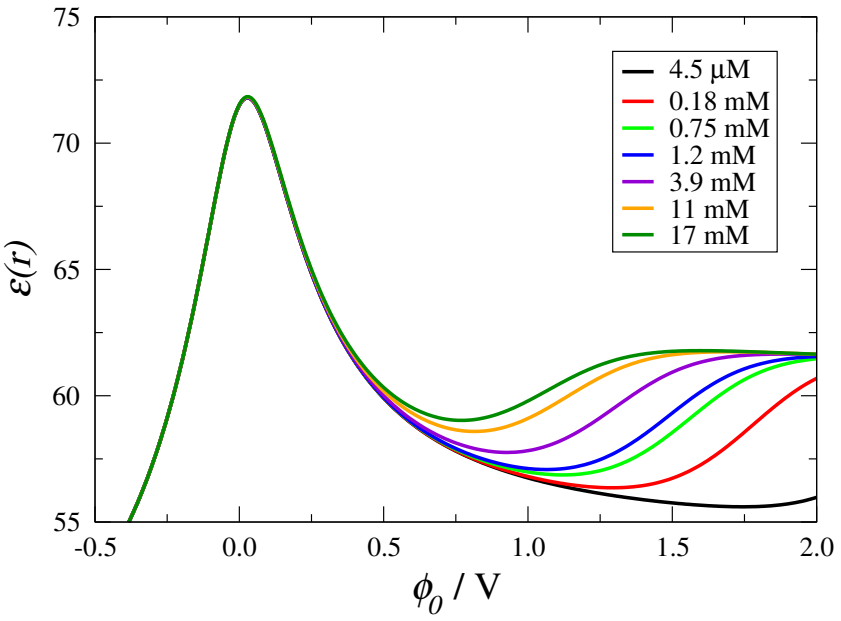

Figure 11. Permittivity at $z = h$ m for the NaF-NaCl EDL as a function of the applied potential.

The aforementioned authors detail how a species with $c^{\max,\mathrm{vol}} < c^{\max,\chi}$ will, when the maximum concentration is reached, reduce the electrolyte permittivity to $\varepsilon_w + 4\pi c^{\max,\mathrm{vol}}$ rather than to $\varepsilon_w/2$, as when the polarizability term sets the maximum concentration of the species. In the case of Cl^- ions, the relative permittivity should reduce to 61 when the maximum concentration is reached, and since this is larger than the dielectric decrement associated with the F^- ions at lower potentials, the permittivity is forced to initially increase and then decay only slowly to the new lower limit.

Such behavior is not guaranteed for all mixed electrolyte systems. For example if both counter-ions have maximum concentrations set by their volumes but the smaller species has a larger polarizability, the displacement of the larger species at large potentials would decrease the permittivity, causing the differential capacitance to drop. More complex still is the case of a mixed electrolyte containing counter-ions of different valencies, because in this case the maximum concentrations of the two species may be defined by different interactions, and how they affect each other is not immediately clear.

5. Conclusions

In this work, we have developed an analytical method to evaluate the differential capacitance of a planar electrode immersed in an electrolyte solution of ions with finite size and excess polarizability. It only requires the solution of a set of algebraic equations, rather than a differential equation, as required by the full theory. The method applies to any general model that treats the electrostatic interactions at the mean-field level and approximates the other interactions with a local density functional.

We analyzed the effects of excluded volume and excess ion polarizability on C_D in both the low and high potential limits, and also compared the predictions to experimental data for a range of systems. At the point of zero charge, both the excluded volume and excess ion polarizability were found to alter C_D. Asymmetries in the size of the co- and counter-ions led to a reduction of C_D relative to the GCS model, while the reduction in bulk electrolyte permittivity due to the presence of polarizable ions caused a further reduction regardless of any asymmetry. Both were found to be able to reverse the growth of C_D at the PZC, although the polarization interaction appears to do this in a manner which agrees

better with measured data.

As well as reducing C_D at the PZC, asymmetries in the ion properties can also cause the single peak of a high concentration differential capacitance curve to shift away from the PZC. The direction of movement was towards potentials in which the smaller or lower polarizability species is the counter-ion. While the magnitude of the shift is underestimated, the qualitative agreement shows that, even at low potentials, ion-ion and ion-solvent interactions can have measurable effects on the system behavior.

In the high potential limit, both ion polarizability and excluded volume lead to an inverse-square root dependence of the differential capacitance on the potential, in agreement with experimental observations. However, the rate of decay predicted by the theory for both is slower than occurs experimentally, suggesting that either the model underestimates the influence of these effects at high potentials (and thereby concentrations) or that additional phenomena begin to dominate the system behavior under these conditions.

We also applied the model to examine electrolytes with two counter-ion species. For a CsCl-$MgCl_2$ electrolyte, we showed that the polarizability interaction is able to provide an explanation for the observed displacement of Mg^{2+} ions by Cs^+ ions at a highly charged surface. However, we were unable to quantitatively fit the model to the measured differential capacitance curve of a NaCl-NaF electrolyte, although the model results did exhibit some of the observed trends, including the emergence of a secondary peak. Despite the lack of quantitative agreement, the model highlights the interplay between the effects of ion excluded volume and polarizability.

Although the model generally compares favorably to experimental data, using only the Stern layer width as a fitting parameter, a number of limitations were identified. The deviations of the model predictions from measured data occur for systems with large bulk electrolyte concentrations or systems at large electrode potentials, both of which cases feature closely packed ions in the EDL. While some of these can be attributed to applying the model to situations in which it is not strictly valid (i.e. $c(\mathbf{r}) \gtrsim 2\,\mathrm{M}$ or $|\phi'| \gtrsim 0.25\,\mathrm{V\,nm^{-1}}$), there remain a number of other unaccounted for effects which will impact the predicted differential capacitance.

The mean field treatment of the electrostatic interactions used in this work neglects correlations between charges, which can play a significant role in determining the EDL structure, particularly for higher valency ions and higher surface charges for large applied potentials. Such correlations lead to a breakdown of the mean-field approximation, and a non-local theory [47, 48] that can account for strong fluctuations in the electrostatic potential is required to improve upon the standard continuum theory [49].

Other effects can influence the EDL structure and thereby contribute towards determining the differential capacitance. We have discussed changes to the solvent permittivity due to the presence of ions, but the electric field itself can also cause a dielectric decrement [50]. In particular, the strong alignment of solvent molecules near the surface at high potentials, and the reduction in permittivity associated with it [51], will contribute to a reduction of the differential capacitance (see Eq. (25)).

We have also neglected specific interactions between the ions and the surface. The importance of these interactions is visible in, for example, the differences between the differential capacitance of the same electrolyte at electrodes made from different materials, or even at different crystal faces of the same electrode material [52]. Polarization of the electrode itself would lead to an "image charge" interaction [47, 48, 53] between it and the ions in the system. This interaction would typically be attractive for all counter-ion and co-ion species, however, its magnitude would depend on properties, such as the polarizability, of the ions. Differences between the surface interaction energies of co- and counter-ions in single electrolytes would contribute to the asymmetry which is responsible for shifting the peak differential capacitance at high concentrations. For mixed electrolytes, asymmetric surface interactions between the two counter-ion species would also

alter the displacement behavior, which would affect the relative shape, position and size of the two peaks.

Acknowledgments

G Minton acknowledges support from the EPSRC DTA.

References

[1] M.Z. Bazant, M.S. Kilic, B.D. Storey and A. Ajdari, Adv. Colloid Interface Sci. **152** (1-2), 48 (2009).
[2] X. Wang, C. Cheng, S. Wang and S. Liu, Microfluid. Nanofluidics **6**, 145 (2009).
[3] B.D. Storey, L.R. Edwards, M.S. Kilic and M.Z. Bazant, Phys. Rev. E **77**, 036317 (2008).
[4] D. Gillespie, W. Nonner and R.S. Eisenberg, J. Phys.: Condens. Matter **14** (46), 12129 (2002).
[5] I. Vlassiouk, S. Smirnov and Z. Siwy, Nano Letters **8** (7), 1978 (2008).
[6] T.L. Horng, T.C. Lin, C. Liu and B. Eisenberg, J. Phys. Chem. B **116** (37), 11422 (2012).
[7] M.Z. Bazant, M.S. Kilic, B.D. Storey and A. Ajdari, Adv Colloid Interface Sci. **152** (1-2), 48 (2009).
[8] M. Gouy, J. Phys. Theor. Appl. **9**, 457 (1910).
[9] D.L. Chapman, Philos. Mag. **25** (148), 475 (1913).
[10] O. Stern, Zeit. Elektrochem **30**, 508 (1924).
[11] J. Bikerman, Philos. Mag. **33** (220), 384 (1942).
[12] P.M. Biesheuvel and M. van Soestbergen, J. Colloid Interf. Sci. **316** (2), 490 (2007).
[13] S. Lamperski, C.W. Outhwaite and L.B. Bhuiyan, J. Phys. Chem. B **113** (26), 8925 (2009).
[14] P. Ballone, G. Pastore and M.P. Tosi, J. Chem. Phys. **85** (5), 2943 (1986).
[15] D. Jiang, D. Meng and J. Wu, Chem. Phys. Lett. **504** (4-6), 153 (2011).
[16] D. Henderson and S. Lamperski, J. Chem. Eng. Data **56** (4), 1204 (2011).
[17] L.B. Bhuiyan, C.W. Outhwaite and D. Henderson, J. Chem. Phys. **123** (3), 034704 (2005).
[18] J. Forsman, C.E. Woodward and M. Trulsson, J. Phys. Chem. B **115** (16), 4606 (2011).
[19] A.A. Kornyshev, J. Phys. Chem. B **111** (20), 5545 (2007).
[20] Y. Lauw, M.D. Horne, T. Rodopoulos, A. Nelson and F.A.M. Leermakers, J. Phys. Chem. B **114** (34), 11149 (2010).
[21] M.V. Fedorov and A.A. Kornyshev, Electrochim. Acta **53** (23), 6835 (2008).
[22] J.B. Hasted, D.M. Ritson and C.H. Collie, J. Chem. Phys. **16** (1), 1 (1948).
[23] D. Ben-Yaakov, D. Andelman, D. Harries and R. Podgornik, J. Phys.: Condens. Matter **21**, 424106 (2009).
[24] S. Gavryushov and P. Linse, J. Phys. Chem. B **107** (29), 7135 (2003).
[25] D. Ben-Yaakov, D. Andelman and R. Podgornik, J. Chem. Phys. **134** (7), 074705 (2011).
[26] M.M. Hatlo, R. van Roij and L. Lue, EPL **97** (2), 28010 (2012).
[27] Y. Nakayama and D. Andelman, J. Chem. Phys. **142** (4), 044706 (2015).
[28] J.J. López-García, J. Horno and C. Grosse, J. Colloid Interface Sci. **380** (1), 213 (2012).
[29] J.J. López-García, J. Horno and C. Grosse, J. Colloid Interface Sci. **405**, 336 (2013).
[30] M.I. Gorenstein, A.P. Kostyuk and Y.D. Krivenko, J. Phys. G **25** (9), L75 (1999).
[31] E.R. Nightingale, J. Phys. Chem. **63** (9), 1381 (1959).
[32] L. Lue, N. Zoeller and D. Blankschtein, Langmuir **15** (11), 3726 (1999).
[33] D. Gillespie, Microfluid. Nanofluidics **18** (5), 717 (2014).
[34] T. Boublik, J. Chem. Phys. **53** (1), 471 (1970).
[35] G.A. Mansoori, N.F. Carnahan, K.E. Starling and T.W. Leland, J. Chem. Phys. **54** (4), 1523 (1971).
[36] M.Z. Bazant, B.D. Storey and A.A. Kornyshev, Phys. Rev. Lett. **106** (4), 046102 (2011).
[37] M. Ammam, D.D. Caprio and L. Gaillon, Electrochim. Acta **61** (0), 207 (2012).
[38] I.C. Yeh and M.L. Berkowitz, J. Chem. Phys. **110** (16), 7935 (1999).
[39] R.P. Joshi, J. Qian, K.H. Schoenbach and E. Schamiloglu, J. Appl. Phys. **96** (7), 3617 (2004).
[40] M.V. Fedorov and A.A. Kornyshev, J. Phys. Chem. B **112** (38), 11868 (2008).
[41] A.A. Kornyshev, J. Phys. Chem. B **111** (20), 5545 (2007).
[42] G. Valette, J. Electroanal. Chem. Interfacial Electrochem. **122** (0), 285 (1981).
[43] A. Hamelin, J. Electroanal. Chem. Interfacial Electrochem. **138** (2), 395 (1982).
[44] V.L. Shapovalov and G. Brezesinski, J. Phys. Chem. B **110** (20), 10032 (2006).
[45] S. Lamperski and C. Outhwaite, J. Colloid Interface Sci. **328** (2), 458 (2008).
[46] D. Larkin, K.L. Guyer, J.T. Hupp and M.J. Weaver, J. Electroanal. Chem. Interfacial Electrochem. **138** (2), 401 (1982).

[47] M.M. Hatlo and L. Lue, Soft Matter **5**, 125 (2009).
[48] M.M. Hatlo and L. Lue, EPL **89** (2), 25002 (2010).
[49] B.D. Storey and M.Z. Bazant, Phys. Rev. E **86**, 056303 (2012).
[50] F. Booth, J. Chem. Phys. **19** (4), 391 (1951).
[51] E. Gongadze, A. Velikonja, Š. Perutkova, P. Kramar, A. Maček-Lebar, V. Kralj-Iglič and A. Iglič, Electrochim. Acta **126**, 42 (2014).
[52] F. Veggini, S. Trasatti and L. Doubova, J. Electroanal. Chem. **378** (12), 125 (1994).
[53] M.M. Hatlo and L. Lue, Soft Matter **4**, 1582 (2008).